*Journal of Sound and Vibration* (1998) **213**(4), 619–641

# ACOUSTIC ATTENUATION PERFORMANCE OF CIRCULAR EXPANSION CHAMBERS WITH OFFSET INLET/OUTLET: II. COMPARISON WITH EXPERIMENTAL AND COMPUTATIONAL STUDIES

A. Selamet, Z. L. Ji and P. M. Radavich

*Department of Mechanical Engineering and The Center for Automotive Research, The Ohio State University, Columbus, OH* 43210-1107, *U.S.A.*

(*Received* 20 *August* 1997, *and in final form* 8 *January* 1998)

This is the second of two papers investigating the acoustic attenuation performance of asymmetric, circular expansion chambers with respect to the chamber length and the relative location of the offset inlet/outlet. Three approaches are employed to determine the transmission loss: (1) the three-dimensional analytical approach developed by the authors in a companion paper (Selamet and Ji, 1998, *Journal of Sound and Vibration* **213,** 601–617) [1]; (2) the three-dimensional computational solution based on the boundary element method; and (3) experiments on an extended impedance tube set-up with expansion chambers fabricated with fixed inlet, outlet, and chamber diameters, varying chamber length to diameter ratios, and varying offset locations of the inlet and outlet. The results from the three approaches are shown to agree well. The effect of geometry, particularly that of the offset angles of the asymmetric configurations, on the multidimensional wave propagation and acoustic attenuation performance is discussed in detail.



## 1. INTRODUCTION

The inlet and outlet locations of the expansion chambers affect the excitation and transmission of higher order modes significantly. This effect of multidimensional wave propagation on the acoustic attenuation performance needs to be considered to obtain accurate predictions for the design of these silencers. Several useful works on the multidimensional wave propagation in expansion chambers have been cited in reference [1], and will not be discussed here with the exception of Eriksson *et al*. [2, 3]. Their experimental investigation on the effect of inlet/outlet locations and the chamber length on transmission loss of the asymmetric expansion chambers is directly relevant to the present study. They have concluded that (1) when the inlet and outlet are offset 180°, the (1, 0) first asymmetric mode is excited and the plane wave behaviour is found only up to the (1, 0) mode; (2) offsetting the inlet and outlet by 90° results in nearly a plane wave behaviour up to the cut-off frequency of the (2, 0) second asymmetric mode; (3) when the outlet axis approaches the pressure nodal circle for the first radial (0, 1) mode, this mode does not appear to be as strongly excited, which results in a plane wave propagation till much higher frequencies in the vicinity of the (2, 0) mode; and (4) as the length is decreased for the short-length chamber with $\theta_0 = 180°$, the transmission loss below the cut-off frequency decreases, and the chamber performance approaches the case of a straight pipe for low frequencies.

0022–460X/98/240619 + 23 $25.00/0/sv981515 

TABLE 1

*Expansion chamber geometry* ($d_1 = d_2 = 4{\cdot}859$ cm, $d = 15{\cdot}318$ cm)

| Geometry | $l$ (cm) | $l/d$ |
|---|---|---|
| 1 | 3·139 | 0·205 |
| 2 | 9·371 | 0·612 |
| 3 | 15·689 | 1·024 |
| 4 | 21·981 | 1·435 |
| 5 | 28·230 | 1·843 |
| 6 | 34·552 | 2·256 |
| 7 | 40·838 | 2·666 |
| 8 | 47·113 | 3·076 |
| 9 | 54·000 | 3·525 |

By combining the acoustic pressure and particle velocity continuity conditions at the inlet and outlet with the orthogonality relations of Fourier–Bessel functions, a three-dimensional analytical approach was developed by the authors to determine the transmission loss of circular expansion chambers with offset inlet and outlet ducts [1]. Two extreme configurations (a short and a long chamber) were considered for illustration purposes, and the transmission loss obtained from the analytical approach was compared with the classical one-dimensional predictions and the earlier multidimensional works.

Numerical techniques, such as the finite element method (FEM) [4–8] and the boundary element method (BEM) [9–11] have also been used to predict the acoustic attenuation performance of mufflers. These methods are usually not restricted by the geometry and can be applied to the acoustic analysis of commercial silencers with complex internal geometry. The advantage of the BEM is that only the boundary surface needs to be discretized, which saves considerable labour as compared with the FEM.

The objective of the present study is to compare the three-dimensional analytical results with the three-dimensional BEM predictions, as well as the experiments on an extended

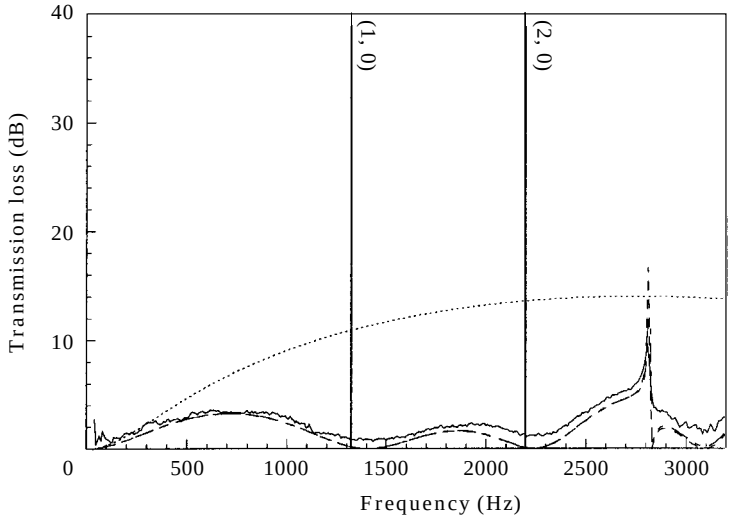


Figure 1. Transmission loss of circular expansion chamber with $l/d = 0{\cdot}205$, $\delta_1 = \delta_2 = 5{\cdot}10$ cm, $\theta_0 = 180°$: ——, experimental; · · · · ·, 1-D analytical; – – –, 3-D analytical; – - –, BEM.

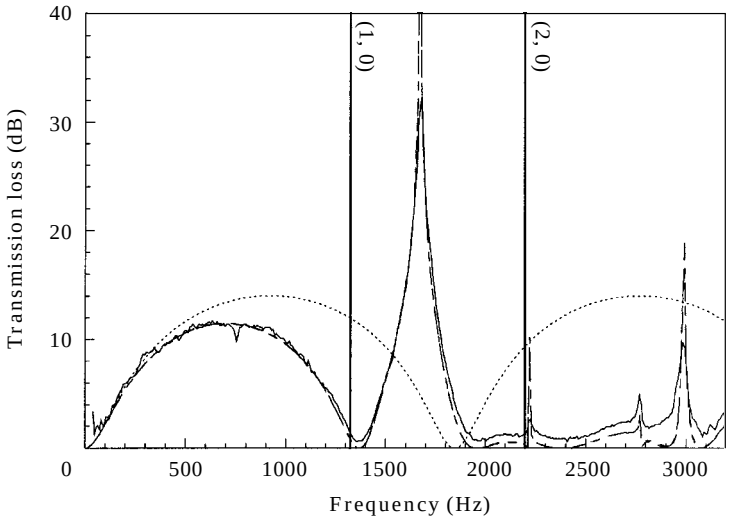


Figure 2. Transmission loss of circular expansion chamber with $l/d = 0{\cdot}612$, $\delta_1 = \delta_2 = 5{\cdot}10$ cm, $\theta_0 = 180^\circ$: ——, experimental; · · · · ·, 1-D analytical; – – –, 3-D analytical; – - –, BEM.

impedance tube set-up. Nine configurations of different lengths were fabricated. The inlet and outlet of each cylindrical chamber are offset and can be rotated to give $\theta_0 = 90^\circ$ and $\theta_0 = 180^\circ$. The justification for the number of configurations was given in an earlier work [12]. While some of the reasons are now different, the same number is retained in the present study to provide a direct comparison of the acoustic attenuation between concentric and asymmetric expansion chambers.

Following the Introduction, the direct BEM and the experimental work are described briefly. The transmission loss results from three approaches are compared next, and the

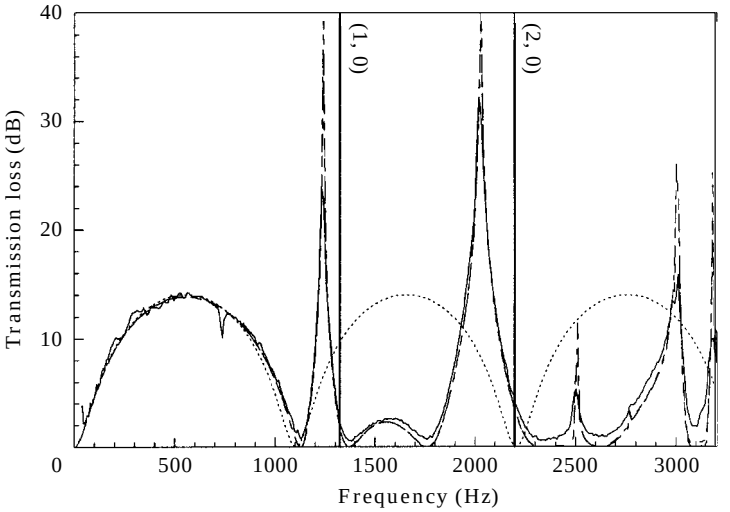


Figure 3. Transmission loss of circular expansion chamber with $l/d = 1{\cdot}024$, $\delta_1 = \delta_2 = 5{\cdot}10$ cm, $\theta_0 = 180^\circ$: ——, experimental; · · · · ·, 1-D analytical; – – –, 3-D analytical; – - –, BEM.

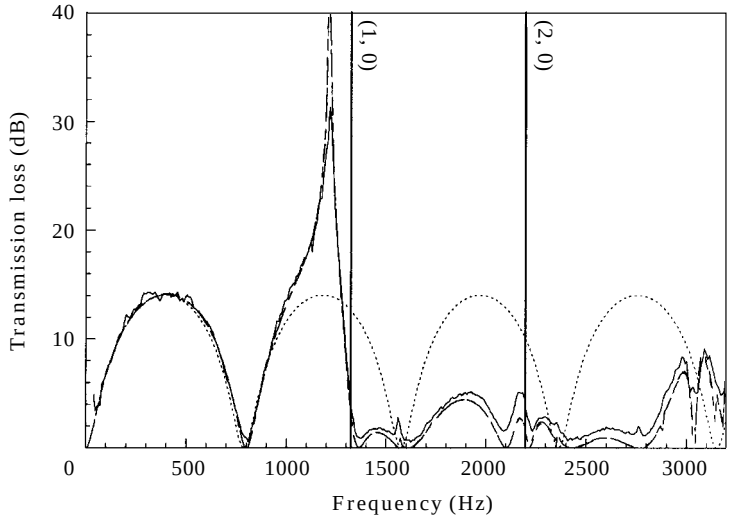


Figure 4. Transmission loss of circular expansion chamber with $l/d = 1{\cdot}435$, $\delta_1 = \delta_2 = 5{\cdot}10$ cm, $\theta_0 = 180^\circ$: ——, experimental; · · · · ·, 1-D analytical; – – –, 3-D analytical; – - –, BEM.

effects of chamber length and inlet/outlet locations on the acoustic attenuation performance of expansion chambers are discussed. The study is concluded with some final remarks.

## 2. BOUNDARY ELEMENT METHOD

The sound propagation in a duct is given by the well-known Helmholz equation as [13]

$$\nabla^2 P + k^2 P = 0, \tag{1}$$

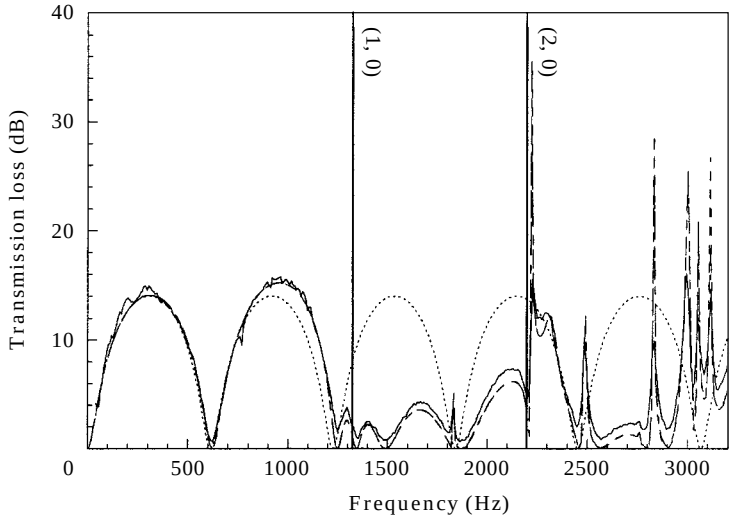


Figure 5. Transmission loss of circular expansion chamber with $l/d = 1{\cdot}843$, $\delta_1 = \delta_2 = 5{\cdot}10$ cm, $\theta_0 = 180^\circ$: ——, experimental; · · · · ·, 1-D analytical; – – –, 3-D analytical; – - –, BEM.

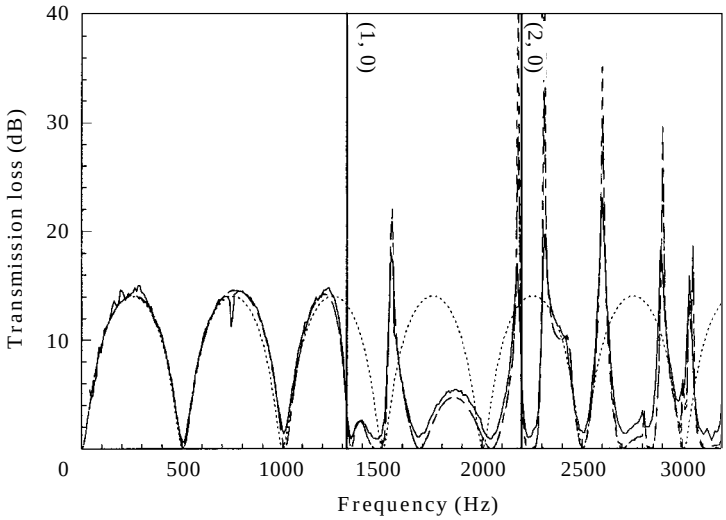


Figure 6. Transmission loss of circular expansion chamber with $l/d = 2{\cdot}256$, $\delta_1 = \delta_2 = 5{\cdot}10$ cm, $\theta_0 = 180^\circ$: ——, experimental; · · · · ·, 1-D analytical; – – –, 3-D analytical; – - –, BEM.

where $P$ is the acoustic pressure, $k = \omega/c$ is the wavenumber, $\omega$ is the angular frequency, and $c$ is the sound speed. The boundary integral equation of this relationship can be represented as [9–11]

$$C(X)P(X) = \int_S \left[ G(X, Y) \frac{\partial P}{\partial \mathbf{n}}(Y) - P(Y) \frac{\partial G}{\partial \mathbf{n}}(X, Y) \right] \mathrm{d}S(Y). \tag{2}$$

Here, $S$ is the boundary surface of the acoustic domain, $\mathbf{n}$ is the unit normal vector on $S$ directed away from the domain, the function $G(X, Y) = \exp(-\mathrm{j}kR)/4\pi R$ is Green's function of free space, where $R = |X - Y|$ is the distance between any two points $X$ and

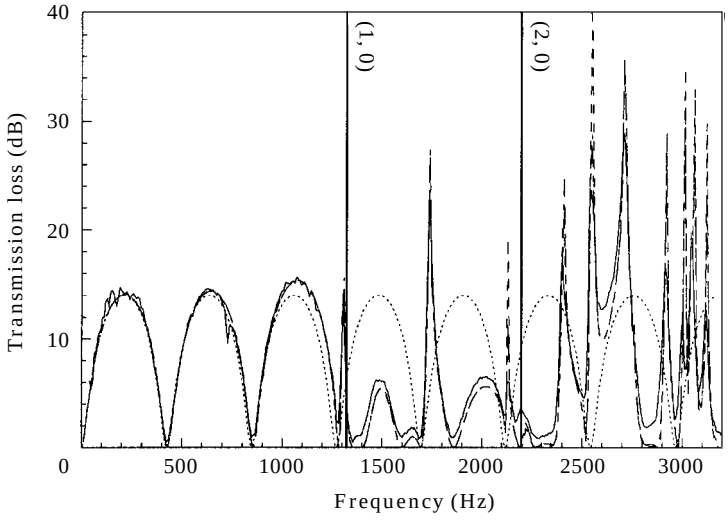


Figure 7. Transmission loss of circular expansion chamber with $l/d = 2{\cdot}666$, $\delta_1 = \delta_2 = 5{\cdot}10$ cm, $\theta_0 = 180^\circ$: ——, experimental; · · · · ·, 1-D analytical; – – –, 3-D analytical; – - –, BEM.

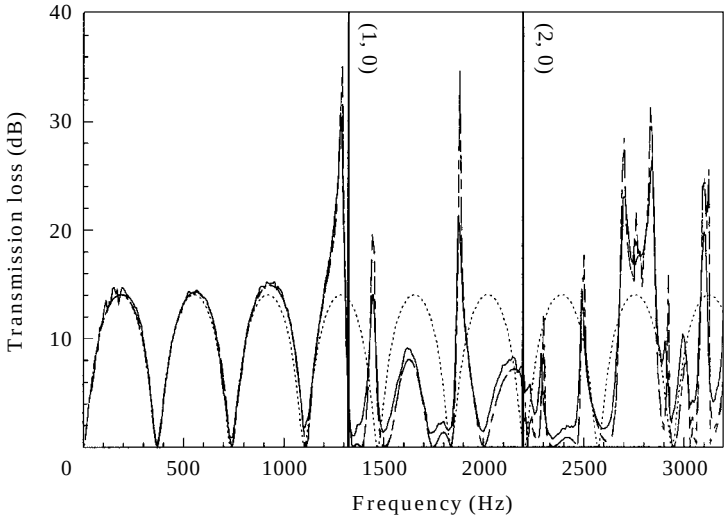


Figure 8. Transmission loss of circular expansion chamber with $l/d = 3{\cdot}076$, $\delta_1 = \delta_2 = 5{\cdot}10$ cm, $\theta_0 = 180^\circ$: ——, experimental; · · · · ·, 1-D analytical; – – –, 3-D analytical; – - –, BEM.

$Y$ in the domain or on the surface, and $C(X)$ is a coefficient which depends on the position of point $X$.

A numerical solution of the boundary integral equation (2) can be achieved by discretizing the boundary surface of the domain into a number of elements. By using discretization and numerical integration, and introducing the momentum equation [13]

$$j\rho\omega\mathbf{U} = -\nabla P, \tag{3}$$

the following algebraic system of equations is obtained:

$$[A]\{P\} = [B]\{U_n\}, \tag{4}$$

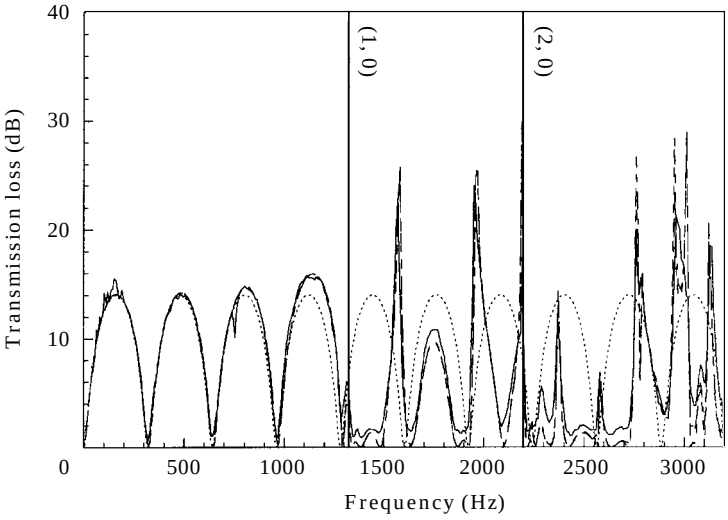


Figure 9. Transmission loss of circular expansion chamber with $l/d = 3{\cdot}525$, $\delta_1 = \delta_2 = 5{\cdot}10$ cm, $\theta_0 = 180^\circ$: ——, experimental; · · · · ·, 1-D analytical; – – –, 3-D analytical; – - –, BEM.

where $[A]$ and $[B]$ are the coefficient matrices, and $\{P\}$ and $\{U_n\}$ are the vectors whose elements are the sound pressure $P$ and outward normal particle velocity $U_n$, on the boundary nodes, respectively.

If either $P$ or $U_n$ is known, or a linear relation between $P$ and $U_n$ is given, equation (4) can be solved. Once the surface values are known, the sound pressure at any interior point can be calculated through discretization of equation (2) by setting $C(X) = 1$. The detailed treatment of the numerical solution procedure for the BEM using quadratic isoparametric elements for three-dimensional muffler analysis can be found elsewhere [9, 11]. Note that the employment of the symmetry and substructure techniques for the analysis of mufflers can reduce the computational time and improve the accuracy as compared to the conventional single-domain BEM [10, 11].

## 3. EXPERIMENTAL APPROACH

The experimental set-up consists of an extended impedance tube configuration, where the expansion chambers are placed between a broad-frequency noise source and an anechoic termination. The two-microphone technique [14, 15] is utilized to separate incident and reflected waves for calculation of the transmission loss across the element, with one microphone pair placed before and the other after the expansion chamber. For further details of the experimental set-up, refer to Selamet *et al*. [16].

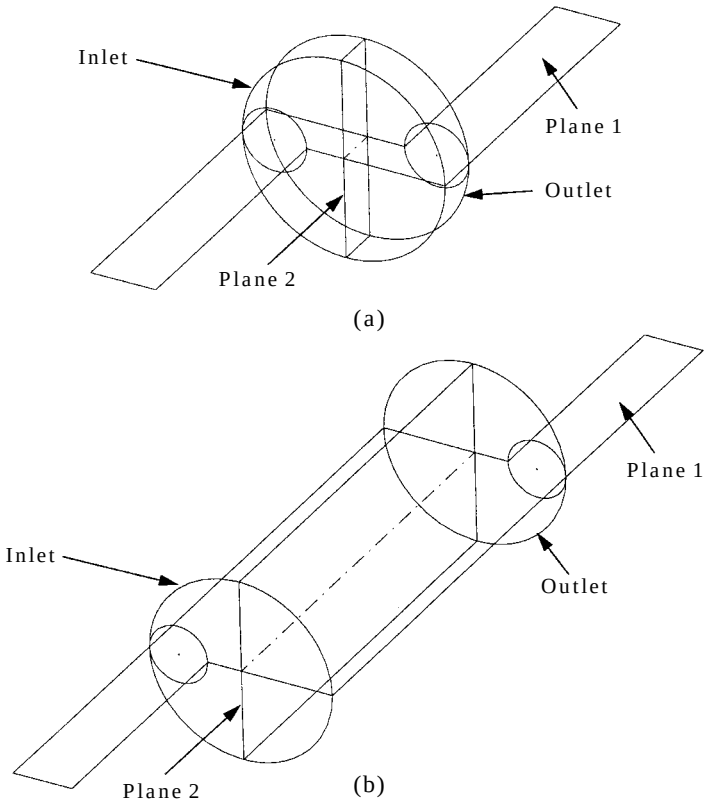


Figure 10. Post-processing planes for expansion chamber with 180° offset: (a) $l/d = 0{\cdot}205$, (b) $l/d = 2{\cdot}256$.

The experimental work is conducted with fabricated expansion chambers at nine different lengths as shown in Table 1. For all configurations, the expansion ratio is held constant, while the chamber length is varied. End caps were built with an offset distance of $\delta = 5{\cdot}10$ cm, and a bolt pattern was selected to allow a relative offset angle of either $\theta_0 = 180^\circ$ or $\theta_0 = 90^\circ$. The speed of sound in the experiments is determined to be 346·1 m/s based on measured air temperature.

## 4. RESULTS AND DISCUSSION

For the nine different lengths given in Table 1 and a relative offset angle 180°, Figures 1–9 compare the transmission loss results from the analytical, computational, and the

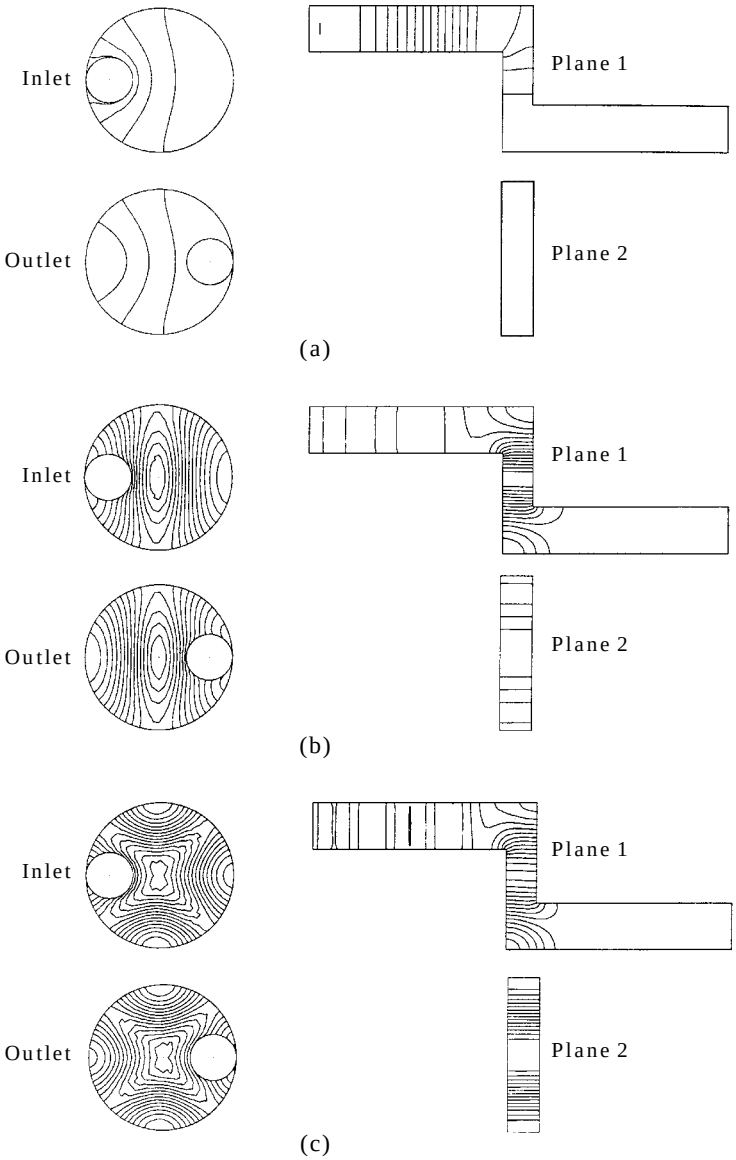


Figure 11. Lines of constant pressure for expansion chamber with 180° offset, $l/d = 0{\cdot}205$ at three frequencies: (a) 500 Hz, (b) 1400 Hz, (c) 2200 Hz.

experimental approaches. These figures show that the results obtained by the analytical and the BEM are nearly identical throughout the frequency range of interest, and also closely match the experimental results. Much of the deviations between these two methods and the experiments, particularly at the sharp resonance peaks, may be attributed to the neglect of viscous damping in the analytical and computational approaches. Figures 3–9 show the (repeating) dome behaviour characteristic of one-dimensional propagation in expansion chambers below the cut-off frequency of the first asymmetric (1, 0) mode. As the $l/d$ ratio of the chamber increases, the number of repeating domes increases, but none

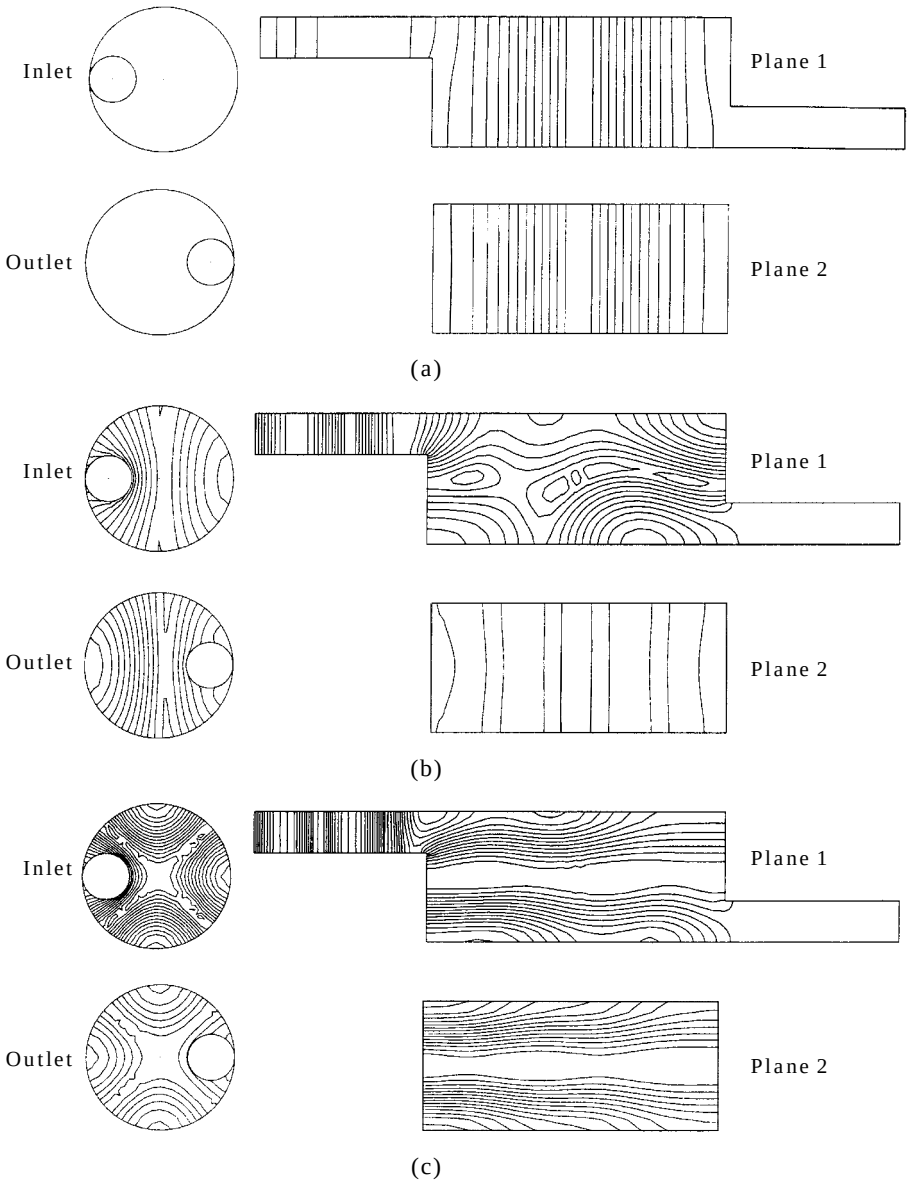


Figure 12. Lines of constant pressure for expansion chamber with 180° offset, $l/d = 2{\cdot}256$ at three frequencies: (a) 500 Hz, (b) 1400 Hz, (c) 2200 Hz.

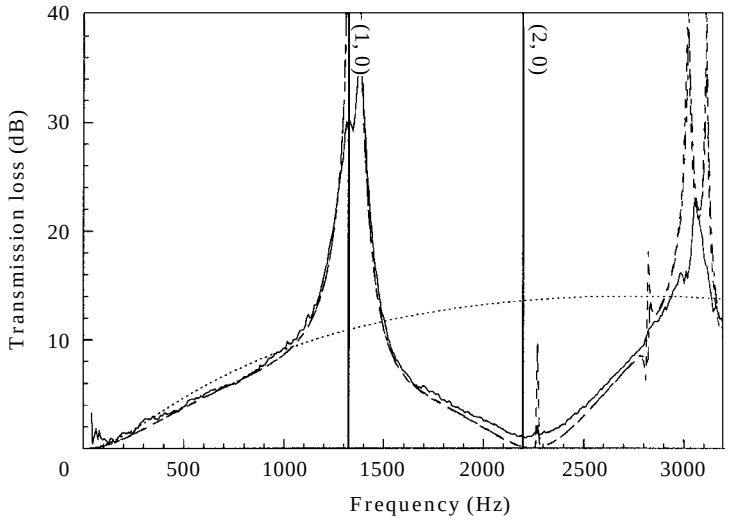


Figure 13. Transmission loss of circular expansion chamber with $l/d = 0{\cdot}205$, $\delta_1 = \delta_2 = 5{\cdot}10$ cm, $\theta_0 = 90^\circ$: ——, experimental; · · · · ·, 1-D analytical; – – –, 3-D analytical; – - –, BEM.

of the domes extends beyond the (1, 0) mode. Above this cut-off frequency, the acoustic attenuation is reduced drastically as the multidimensional propagation begins to dominate. Thus, for the one-dimensional domes, the cut-off frequency for a given mode in a circular duct [1],

$$f < \frac{c}{2\pi}\left(\frac{\alpha_{mn}}{a}\right), \tag{5}$$

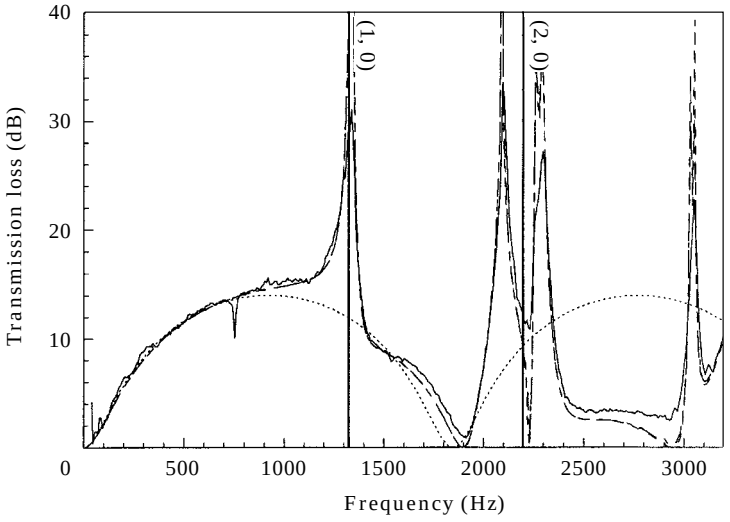


Figure 14. Transmission loss of circular expansion chamber with $l/d = 0{\cdot}612$, $\delta_1 = \delta_2 = 5{\cdot}10$ cm, $\theta_0 = 90^\circ$: ——, experimental; · · · · ·, 1-D analytical; – – –, 3-D analytical; – - –, BEM.

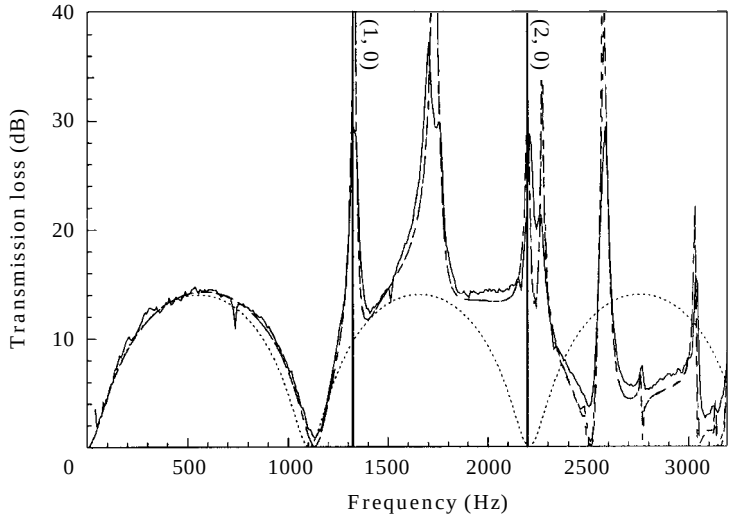


Figure 15. Transmission loss of circular expansion chamber with $l/d = 1{\cdot}024$, $\delta_1 = \delta_2 = 5{\cdot}10$ cm, $\theta_0 = 90^\circ$: ——, experimental; · · · · ·, 1-D analytical; – – –, 3-D analytical; – - –, BEM.

can be rearranged to provide a relationship between the $l/d$ ratio of the chamber and the number of repeating domes, $kl/\pi$, before higher order modes begin to dominate, as

$$\frac{kl}{\pi} < \frac{2\alpha_{mn}}{\pi}\left(\frac{l}{d}\right). \tag{6}$$

The number of domes can then be approximated for the 180° offset expansion chamber by introducing $\alpha_{10} = 1{\cdot}841$ (corresponding to $f_{10} = 1324$ Hz) into equation (6). This suggests that geometries with an $l/d$ ratio of less then 0·853 will have no complete plane wave domes, one dome for $l/d = 0{\cdot}854$–$1{\cdot}706$, two domes for $l/d = 1{\cdot}707$–$2{\cdot}560$, three domes for $l/d = 2{\cdot}561$–$3{\cdot}413$, and four domes for $l/d = 3{\cdot}414$–$4{\cdot}266$. These values show

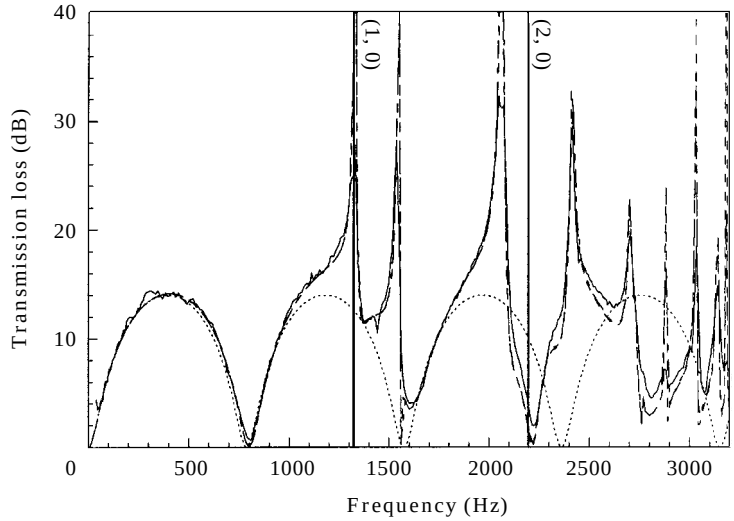


Figure 16. Transmission loss of circular expansion chamber with $l/d = 1{\cdot}435$, $\delta_1 = \delta_2 = 5{\cdot}10$ cm, $\theta_0 = 90^\circ$: ——, experimental; · · · · ·, 1-D analytical; – – –, 3-D analytical; – - –, BEM.

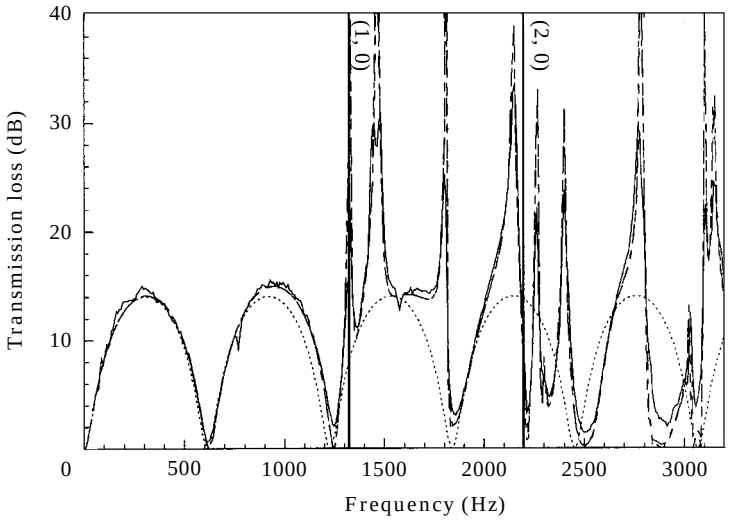


Figure 17. Transmission loss of circular expansion chamber with $l/d = 1{\cdot}843$, $\delta_1 = \delta_2 = 5{\cdot}10$ cm, $\theta_0 = 90^\circ$: ——, experimental; · · · · ·, 1-D analytical; – – –, 3-D analytical; – - –, BEM.

good agreement with the actual number of domes in Figures 3 through 9. The two configurations with $l/d < 0{\cdot}853$ in Figures 1 and 2 show some dome-like behaviour below the first asymmetric (1, 0) mode, but the transmission loss is less than that of the one-dimensional predictions of approximately 14 dB at the dome peaks.

In order to gain further understanding of the effects of higher order mode propagation in these 180° offset expansion chambers, the BEM was used to solve for the pressure contours on two internal planes and two surface planes (the inlet and outlet) for the $l/d = 0{\cdot}205$ and $l/d = 2{\cdot}256$ configurations, as shown in Figure 10. Contours for these two configurations at three frequencies, 500, 1400 and 2200 Hz, are given in Figures 11 and 12. The first frequency is well below the onset of any higher order modes, the second

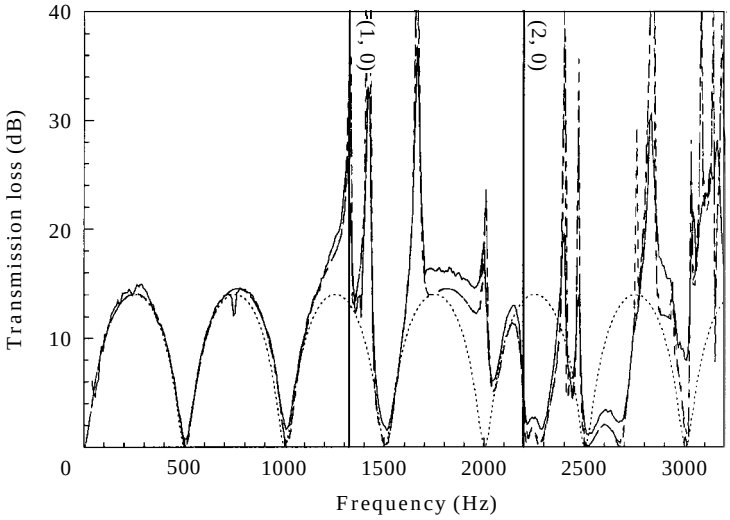


Figure 18. Transmission loss of circular expansion chamber with $l/d = 2{\cdot}256$, $\delta_1 = \delta_2 = 5{\cdot}10$ cm, $\theta_0 = 90^\circ$: ——, experimental; · · · · ·, 1-D analytical; – – –, 3-D analytical; – - –, BEM.

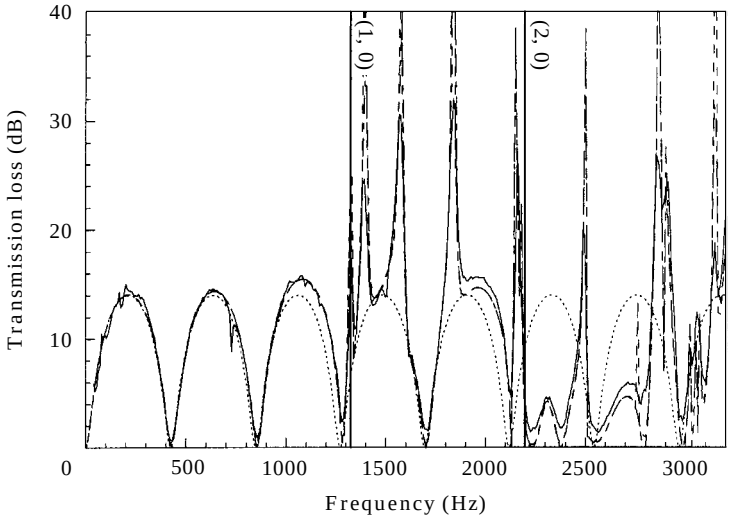


Figure 19. Transmission loss of circular expansion chamber with $l/d = 2{\cdot}666$, $\delta_1 = \delta_2 = 5{\cdot}10$ cm, $\theta_0 = 90^\circ$: ——, experimental; · · · · ·, 1-D analytical; – – –, 3-D analytical; – - –, BEM.

frequency is slightly beyond the cut-off frequency for the (1, 0) mode, and the third frequency is near the (2, 0) mode. For the short $l/d = 0{\cdot}205$ chamber at 500 Hz (Figure 11(a)), multidimensional waves excited at the inlet discontinuity do not have sufficient distance to decay over the length of the chamber, leaving a nearly one-dimensional wave front propagating mainly in the transverse direction in the chamber. It is this approximately planar propagation along the diameter of the chamber that produces the dome-like behaviour of the short expansion chambers in Figures 1 and 2. The reduced transmission loss value of these domes (compared to the 14 dB in Figures 3–9) is due to the smaller effective expansion ratio (now in the transverse direction) of this short chamber. As the wave turns the corner and heads across the diameter of the chamber, it sees an

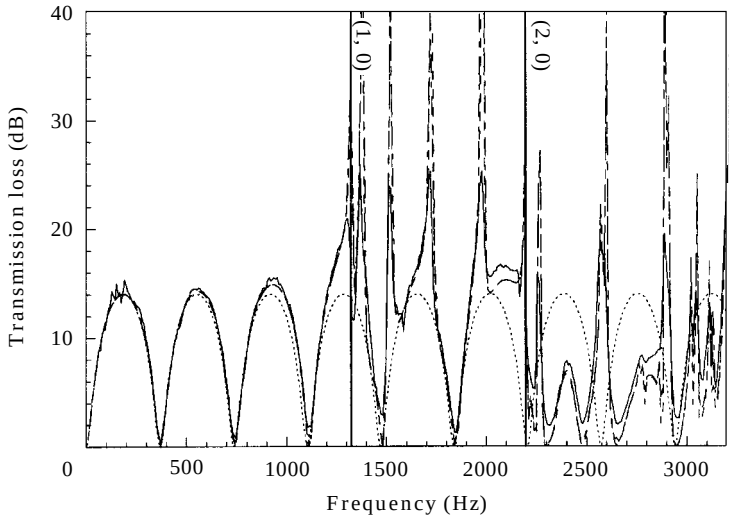


Figure 20. Transmission loss of circular expansion chamber with $l/d = 3{\cdot}076$, $\delta_1 = \delta_2 = 5{\cdot}10$ cm, $\theta_0 = 90^\circ$: ——, experimental; · · · · ·, 1-D analytical; – – –, 3-D analytical; – - –, BEM.

expansion ratio that increases up to the centre of the chamber and then decreases from the centre of the chamber to the outlet. As the length of the chamber is increased in Figure 2, this effective expansion ratio increases resulting in a greater attenuation than that of Figure 1. At 1400 Hz, when the first diametral mode begins to propagate, the short chamber length tends to retain a one-dimensional wave front along the diameter of the chamber, as observed on plane 1 (Figure 11(b)). As the frequency is increased to 2200 Hz, the wave propagation in the transverse direction (plane 2) becomes stronger, and the nearly one-dimenisonal wave propagation begins to fail (Figure 11(c)). At 500 Hz, the longer $l/d = 2{\cdot}256$ configuration (Figure 12(a)) demonstrates nearly one-dimensional wave propagation throughout the chamber, with some slight non-planar bending near the inlet and outlet. As the frequency is increased, the first and second diametral modes begin to propagate in the chamber.

As Eriksson [2] demonstrated, the detrimental effect of the asymmetric mode (1, 0) observed in Figures 3–9 could partially be eliminated by rotating the outlet 90°, thus setting $\theta_0 = 90°$. Figures 13–21 then consider the same nine configurations, now with $\theta_0 = 90°$. These figures again illustrate a good agreement among the analytical approach, BEM, and the experiments. As expected, the transmission loss increases, in general, over the 180° case for all nine configurations, particularly in the frequency band between the (1, 0) and (2, 0) modes. Figures 15–21 show the familiar one-dimensional domes up until the cut-off frequency for the (1, 0) mode, where a sharp peak occurs. Careful observation of these figures reveals that, however, by ignoring the numerous peaks, the repeating dome behaviour continues with reasonable accuracy up until the (2, 0) mode begins to propagate. Thus, for the 90° offset chamber, substituting $\alpha_{20} = 3{\cdot}054$ (corresponding to $f_{20} = 2196$ Hz) into equation (6) predicts $l/d = 0{\cdot}514$ for transition, suggesting no one-dimensional dome for Figure 13, one dome for Figure 14, approximately two domes for Figure 15 (this is a borderline case between one and two domes), two domes for Figure 16, three domes for Figure 17, four domes for Figure 18, five domes for Figure 19, approximately six domes for Figure 20 (again a borderline case between five and six domes), and six domes for Figure 21. Comparison with Figures 13–21 suggests that this is a reasonable estimate.

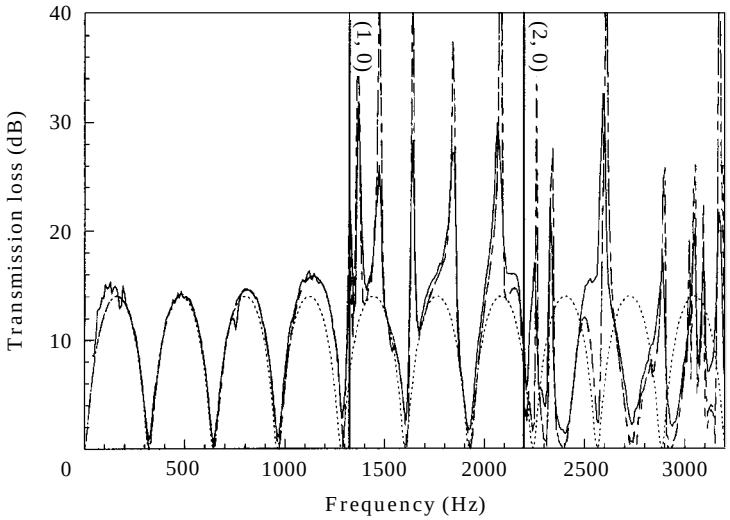


Figure 21. Transmission loss of circular expansion chamber with $l/d = 3{\cdot}525$, $\delta_1 = \delta_2 = 5{\cdot}10$ cm, $\theta_0 = 90°$: ——, experimental; · · · · ·, 1-D analytical; – – –, 3-D analytical; – - –, BEM.

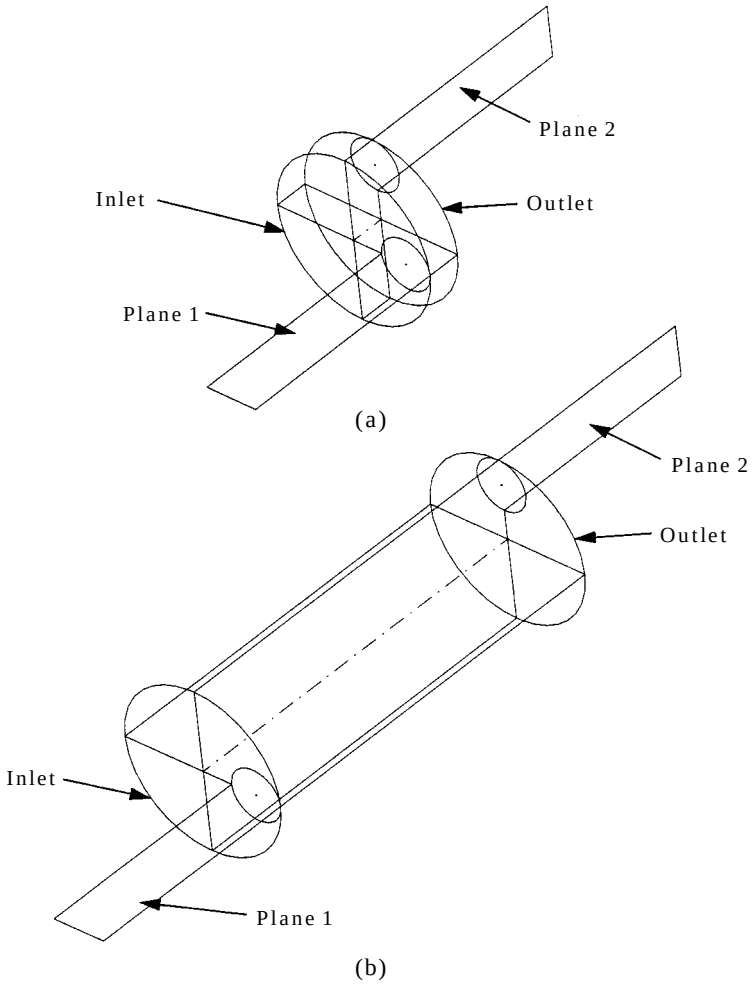


Figure 22. Post-processing planes for expansion chamber with 90° offset: (a) $l/d = 0{\cdot}205$, (b) $l/d = 2{\cdot}256$.

To determine the true extent of higher order modes, the BEM was again used to solve for the pressure contours on the inlet and outlet surfaces and on two internal planes for the $l/d = 0{\cdot}205$ and $l/d = 2{\cdot}256$ configurations, as shown in Figure 22. Contours for these two $l/d$ ratios at frequencies of 500, 1400 and 2200 Hz are given in Figures 23 and 24. At 500 Hz, the short $l/d = 0{\cdot}205$ configuration again allows for multidimensional wave propagation at the transitions and creates nearly one-dimensional wave propagation in the transverse direction (Figure 23(a)). At 1400 Hz, which is near the resonance frequency of Figure 13, the one-dimensional diametral propagation causes the chamber to behave more like a quarter wave resonator (Figure 23(b)). Waves from the inlet travel along the diameter and reflect from the opposite side of the chamber. The outlet is located at a pressure nodal line at this frequency, and does not have an impact on the resonance. As the frequency is increased to 2200 Hz for this short chamber (Figure 23(c)), the wave propagation in the outlet plane (plane 2) becomes stronger and disrupts the one-dimensional type resonance. For the long chamber with $l/d = 2{\cdot}256$, Figure 24(a) shows nearly planar propagation at 500 Hz, with some multidimensional effects near the

inlet and outlet. At the higher frequency of 1400 Hz, the first diametral (1, 0) mode propagates, creating non-planar wave fronts in the expansion chamber (Figure 24(b)). Thus, even though the transmission loss continues to exhibit a one-dimensional type behaviour in Figure 18, it is not due to the fact that the outlet location is delaying the onset of the (1, 0) mode. The outlet at this frequency is located on a nodal line, however, which makes it less dependent on the propagating (1, 0) mode. The increase in frequency to 2200 Hz then excites the second diametral (2, 0) mode (Figure 24(c)). These trends are further illustrated in Figure 25 which shows the contributions from each term in the summation for equations (13)–(19), (21) and (25)–(32) of reference [1] leading to transmission loss. The effect of $q$-terms is negligible until about 2700 Hz for this configuration, thus only $p$ is varied, while setting $q = 0$. As expected, the (0, 0) term is sufficient within about few hundred Hz of the first diametral mode. Similarly, the addition

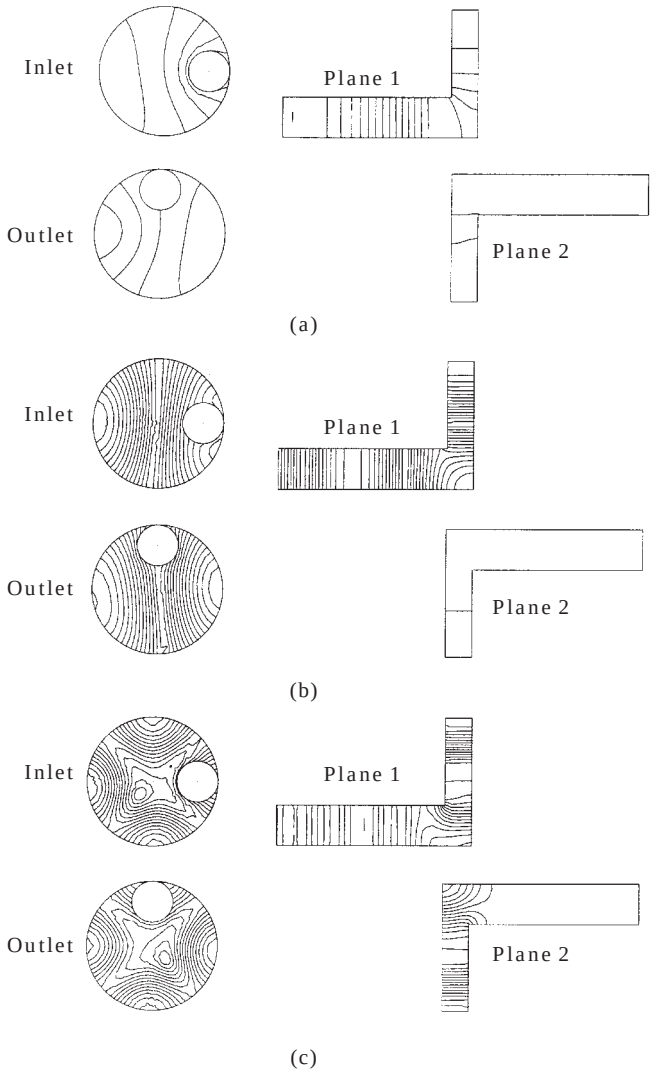


Figure 23. Lines of constant pressure for expansion chamber with 90° offset, $l/d = 0{\cdot}205$ at three frequencies: (a) 500 Hz, (b) 1400 Hz, (c) 2200 Hz.

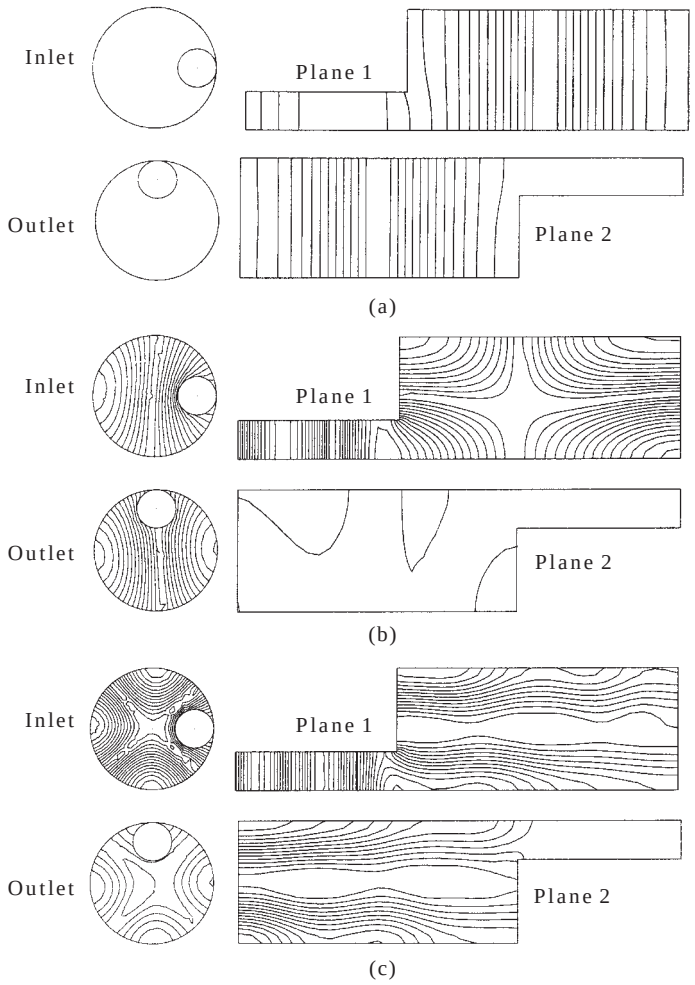


Figure 24. Lines of constant pressure for expansion chamber with 90° offset, $l/d = 2{\cdot}256$ at three frequencies: (a) 500 Hz, (b) 1400 Hz, (c) 2200 Hz.

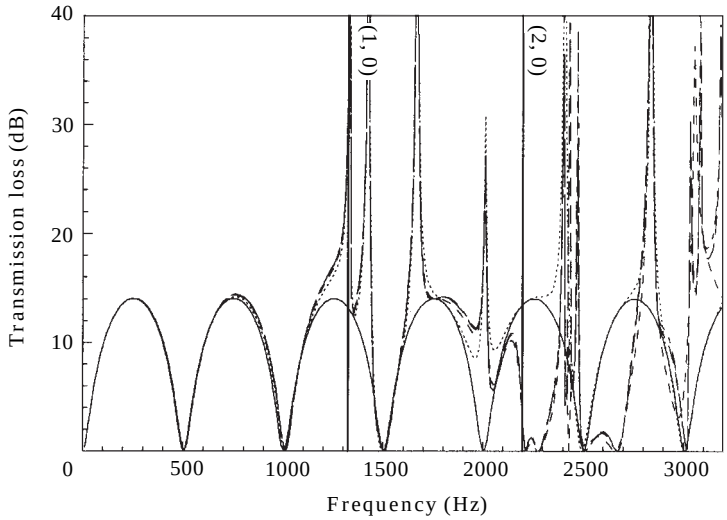


Figure 25. Effect of $p$-terms on transmission loss of circular expansion chamber with $l/d = 2{\cdot}256$, $\delta_1 = \delta_2 = 5{\cdot}10$ cm, $\theta_0 = 90°$: ——, $p = 0$, $q = 0$; · · · · ·, $p = 1$, $q = 0$; - - - -, $p = 2$, $q = 0$; – –, $p = 3$, $q = 0$; – - –, $p = 4$, $q = 0$.

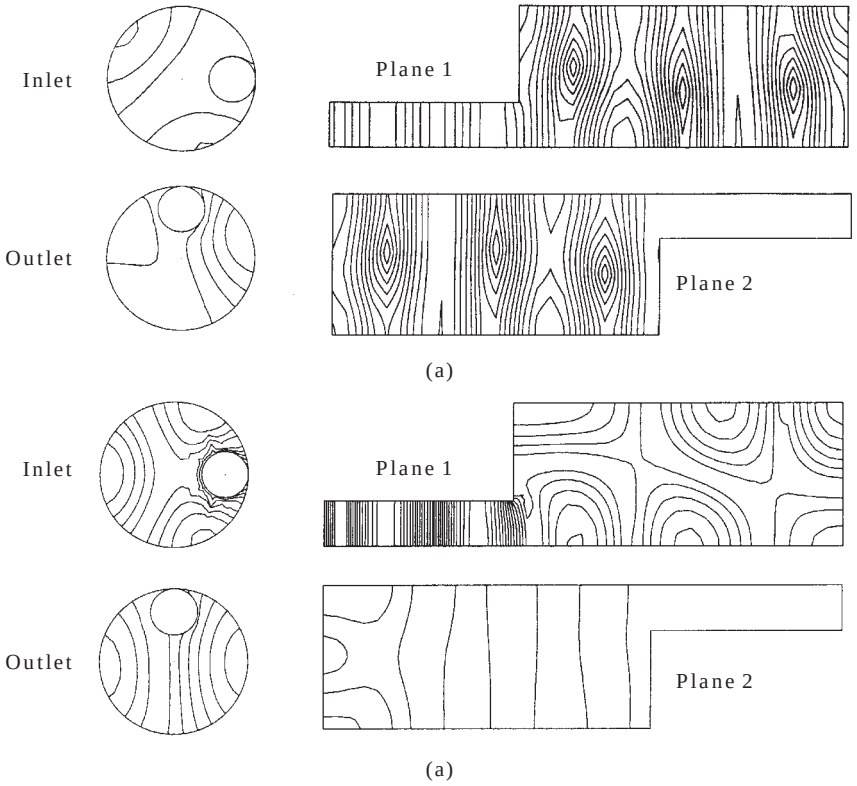


Figure 26. Lines of constant pressure for expansion chamber with 90° offset, $l/d = 2{\cdot}256$ at two frequencies: (a) 1500 Hz, (b) 1800 Hz.

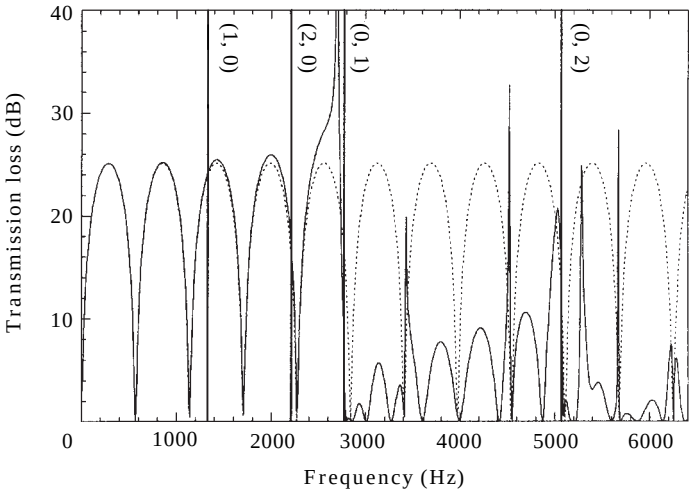


Figure 27. Transmission loss of circular expansion chamber with concentric inlet and concentric outlet: ——, 3-D analytical; · · · · ·, 1-D analytical.

of the (1, 0) term (first diametral contribution) appears to capture the behaviour well prior to the second diametral mode. Near and above this latter mode, the addition of the (2, 0) term appears to be adequate. These analytical observations are consistent with the BEM results of Figure 24. The analytical results also illustrate that near certain frequencies, for example, 1500 Hz, 1800 Hz, etc. (within (1, 0) mode propagation), the effect of terms higher than (0, 0) would almost diminish from a transmission loss standpoint. This fact is illustrated in the contour plots of Figure 26 for these two frequencies.

The expansion chambers with concentric inlet and outlet have been investigated in detail analytically, computationally and experimentally by Selamet *et al*. [6]. For concentric configurations, the first non-planar excitation is due to the (0, 1) first radial mode and the number of plane wave domes can be determined by introducing $\alpha_{01} = 3{\cdot}832$ (corresponding

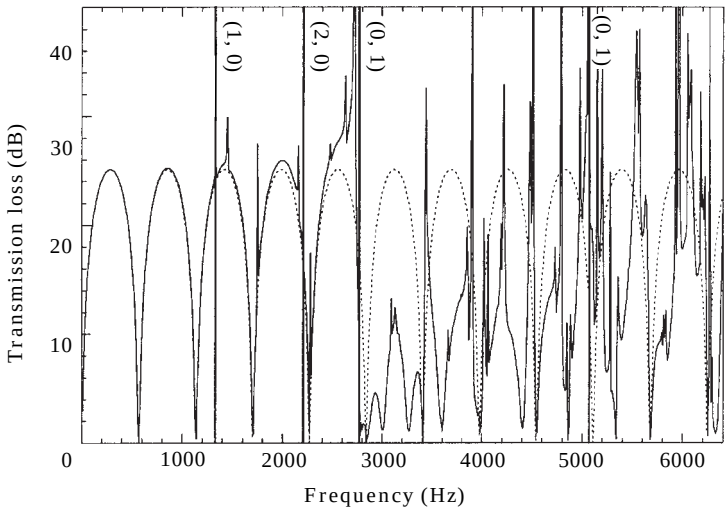


Figure 28. Transmission loss of circular expansion chamber with concentric inlet and offset outlet of 2·60 cm: ——, 3-D analytical; · · · · ·, 1-D analytical.

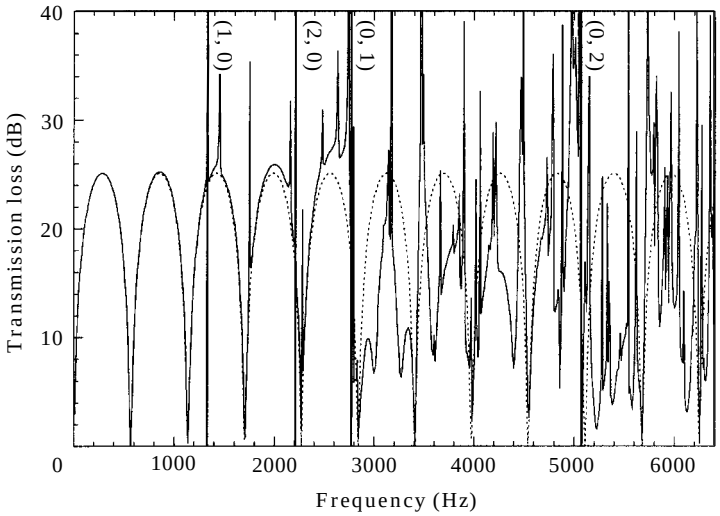


Figure 29. Transmission loss of circular expansion chamber with concentric inlet and offset outlet of 3·85 cm: ——, 3-D analytical; · · · · ·, 1-D analytical.

to $f_{01} = 2756$ Hz for the present configurations) in equation (6). By centring the inlet and offsetting the outlet suitably, the acoustic attenuation performance can be improved, resulting in an effective plane wave propagation inside the expansion chamber until much higher frequencies. To investigate this aspect in more detail, the present three-dimensional analytical aproach is applied to one of the expansion chambers considered by Eriksson (reference [2]: Figure 1(c); chamber length = 12 in., chamber diameter = 6 in., inlet and outlet diameter = 1 in.). By gradually increasing the outlet offset towards the pressure nodal circle of the (0, 1) mode, while maintaining the centred inlet, the acoustic attenuation performance is improved as illustrated in Figures 27–30, particularly in the frequency range between the (0, 1) and (0, 2) modes. Offsetting the outlet by a radial distance of 0·6276

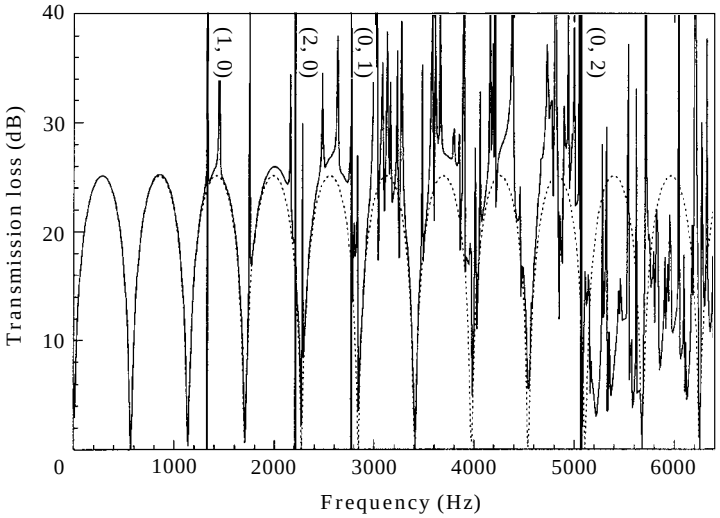


Figure 30. Transmission loss of circular expansion chamber with concentric inlet and offset outlet of 4·78 cm (=0·6276a): ——, 3-D analytical; · · · · ·, 1-D analytical.

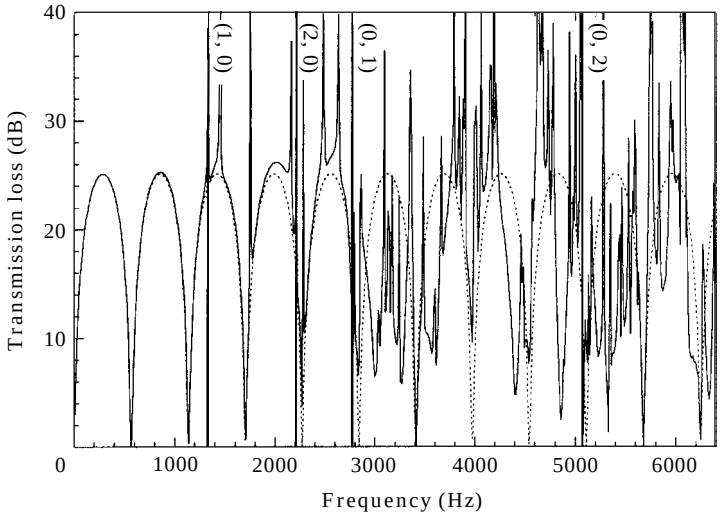


Figure 31. Transmission loss of circular expansion chamber with concentric inlet and offset outlet of 6·35 cm: ——, 3-D analytical; · · · · ·, 1-D analytical.

times the radius of the chamber (the pressure nodal circle of the (0, 1) mode) maximizes the acoustic attenuation performance and extends the effective attenuation band to the (0, 2) mode cut-off frequency (corresponding to $f_{02} = 5072$ Hz for this configuration). Figure 31 represents the case with radial distance slightly beyond the nodal circle. These analytical predictions are consistent with the experimental observations of Eriksson [2]. The foregoing characteristics may also be illustrated analytically for the expansion ratios and lengths used in the present study. Further elaboration is avoided here, however, due to space concerns.

## 5. CONCLUDING REMARKS

The present experimental and computational study is conducted to validate the analytical approach presented in reference [1]. All three aproaches show good agreement for nine fabricated configurations with the relative offset angles of 90° and 180°. The effect of the chamber length and the inlet/outlet positions on the acoustic attenuation performance of expansion chambers are investigated in detail. For the 180° offset expansion chambers with $l/d > 0{\cdot}853$, the repeating one-dimensional (axial) dome behaviour appears below the cut-off frequency of the first diametral (1, 0) mode, while the acoustic attenuation is reduced drastically above this frequency. The configurations with $l/d < 0{\cdot}853$ also exhibit a dome-like behaviour below the (1, 0) mode, however the propagation is now nearly planar in the transverse direction rather than the axial one. Due to the smaller effective expansion ratio in the transverse direction in these configurations, the transmission loss is reduced relative to that of the axial one-dimensional predictions. Rotating the outlet such that $\theta_0 = 90°$ may improve the acoustic attenuation and extends the effective frequency band to the (2, 0) second diametral mode. The expansion chambers of $l/d > 0{\cdot}514$ show the repeating, approximately one-dimensional dome behaviour, while the short chamber of $l/d < 0{\cdot}514$ reveals a dominant resonant peak, resembling a quarter wave resonator. For the expansion chambers with concentric inlet, the effective acoustic attenuation frequency band is also stretched from (0, 1) to the (0, 2) radial mode by offsetting the outlet by a radial distance of 0·6276 times the chamber radius, which

demonstrates the benefit of the concentric inlet and offset outlet arrangement in the muffler design. All of these conclusions are also in agreement with the earlier experimental work of Eriksson and coworkers [2, 3], which provided a direction for the analysis presented here. The combination of the present study with reference [1] is hoped to bring further insight into the interesting attenuation behaviour of the expansion chambers with offset inlet and outlet.

## REFERENCES


1. A. Selamet and Z. L. Ji 1997 *Journal of Sound and Vibration* **213,** 601–617. Acoustic attenuation performance of circular expansion chambers with offset inlet/outlet: I. Analytical approach.
2. L. J. Eriksson 1981 *Proceedings of NOISE-CON*81, *Raleigh*, NC, 105–110. Design implications of higher order mode propagation in silencers.
3. L. J. Eriksson, C. A. Anderson, R. H. Hoops and K. Jayaraman 1983 *Proceedings of* 11*th ICA*, *Paris*, 329–332. Finite length effects on higher order mode propagation in silencers.
4. C.-I. J. Young and M. J. Crocker 1975 *Journal of the Acoustical Society of America* **57**, 144–148. Prediction of transmission loss in mufflers by the finite-element method.
5. A. Craggs 1976 *Journal of Sound and Vibration* **48**, 377–392. A finite element method for damped acoustic systems: an application to evaluate the performance of reactive mufflers.
6. D. F. Ross 1980 *Journal of Sound and Vibration* **69**, 509–518. A finite element method analysis of parallel-coupled acoustic systems using subsystems.
7. A. D. Sahasrabudhe, S. A. Ramu and M. L. Munjal 1991 *Journal of Sound and Vibration* **147**, 371–394. Matrix condensation and transfer matrix techniques in the 3-D analysis of expansion chamber mufflers.
8. A. D. Sahasrabudhe, M. L. Munjal and S. A. Ramu 1992 *Noise Control Engineering Journal* **38**, 27–38. Design of expansion chamber mufflers incorporating 3-D effects.
9. A. F. Seybert and C. Y. R. Cheng 1987 *Journal of Vibration*, *Acoustics*, *Stress*, *and Reliability in Design* **109**, 15–21. Application of the boundary element method to acoustic cavity response and muffler analysis.
10. C. Y. R. Cheng and A. F. Seybert 1991 *Journal of Sound and Vibration* **151**, 119–129. A multidomain boundary element solution for silencer and muffler performance prediction.
11. Z. L. Ji, Q. Ma and Z. H. Zhang 1994 *Journal of Sound and Vibration* **173**, 57–71. Application of the boundary element method to predicting acoustic performance of expansion chamber mufflers with mean flow.
12. A. Selamet and P. M. Radavich 1997 *Journal of Sound and Vibration* **201**, 407–426. The effect of length on the acoustic attenuation performance of concentric expansion chambers: an analytical, computational, and experimental investigation.
13. M. L. Munjal 1987 *Acoustics of Ducts and Mufflers*. New York: Wiley-Interscience.
14. *American Society for Testing and Materials* 1990 *ASTM E* 1050–90, *Philadelphia*, *PA*. Standard test method for impedance and absorption of acoustical materials using a tube, two microphones and a digital frequency analysis system.
15. J. Y. Chung and D. A. Blaser 1980 *Journal of the Acoustical Society of America* **68**, 907–913. Transfer function method of measuring in-duct acoustic properties: I Theory.
16. A. Selamet, N. S. Dickey and J. M. Novak 1994 *Journal of the Acoustical Society of America* **96**, 3177–3185. The Herschel–Quincke tube: a theoretical, computational, and experimental investigation.


## APPENDIX: NOMENCLATURE

| | |
|---|---|
| $a$ | radius of expansion chamber |
| $A, B$ | coefficient matrices |
| $c$ | speed of sound |
| $d, d_1, d_2$ | diameter of expansion chamber, inlet and outlet ducts |
| $f$ | frequency |
| $G$ | $=\exp(-\mathrm{j}kR)/4\pi R$, Green's function |
| $k$ | wavenumber |
| $l$ | length of expansion chamber |

| | |
|---|---|
| $\mathbf{n}$ | unit normal vector |
| $P$ | acoustic pressure |
| $R$ | distance between $X$ and $Y$ |
| $S$ | boundary surface |
| $TL$ | transmission loss |
| $U$ | particle velocity |
| $X$ | interior or surface point |
| $Y$ | surface point |
| $\alpha_{mn}$ | zeros of $J'_m(\alpha_{mn}) = 0$ |
| $\delta_1, \delta_2$ | inlet and outlet offset distances from the centre of chamber |
| $\theta_0$ | relative angle between inlet and outlet |
| $\rho$ | medium density |
| $\omega$ | angular frequency |